JTTEE5 8:447-453

Thermal Barrier Coating Application of Zircon Sand

P. Ramaswamy, S. Seetharamu, K.B.R. Varma, and K.J. Rao

(Submitted 8 June 1998; in revised form 8 January 1999)

Naturally occurring zircon sand was plasma spray coated on steel substrates previously coated with Ni-CrAlY bond coat. The coatings were characterized for their microstructure, chemical composition, thermal shock resistance, and the nature of structural phases present. The as-sprayed coatings consisted of t-ZrO_2 (major phase), m-ZrO_2, $ZrSiO_4$ (minor phases), and amorphous SiO_2. These coatings, when annealed at 1200 °C/1.44 × 10^4 s yielded a $ZrSiO_4$ phase as a result of the reaction between ZrO_2 and SiO_2. Dramatic changes occurred in the characteristics of the coatings when a mixture of zircon sand and Y_2O_3 was plasma spray coated and annealed at 1400 °C/1.44 × 10^4 s. The t-ZrO_2 phase was completely stabilized, and these coatings were found to have considerable potential for thermal barrier applications.

Keywords plasma spray, stabilized ZrO_2, thermal barrier coating, thermal shock resistance, zircon sand

1. Introduction

Zircon is available naturally in the form of sands in the vast beaches of Kerala (southwestern state of India), washed by the Arabian Sea. The chemical analysis of the sand indicates that the sand is composed of zirconium silicate ($ZrSiO_4$) (major phase) with minor impurities of hafnia (HfO_2), alumina (Al_2O_3), magnesia (MgO), calcia (CaO), and iron oxide (Fe_2O_3). Zircon sand is used as a refractory material for making glazes and enamels and also as raw material in the preparation of electrotechnical ceramics (Ref 1). However, to the best of the authors knowledge, there has been very little reported work on plasma sprayed zircon coatings. It is known that zircon decomposes into zirconia (ZrO_2) and silica (SiO_2) when plasma sprayed (Ref 2-5). While Ault (Ref 3) reported the presence of c-ZrO_2 in a siliceous glassy matrix obtained from flame spraying a rod of zircon, Chraska et al. (Ref 4) observed the presence of the three modifications of zirconia (c, m, and t-ZrO_2) along with the glassy SiO_2 phase on plasma spraying of zircon. It has been established that the cooling rate determines whether t-ZrO_2 or c-ZrO_2 is formed in the sprayed coating.

Investigations on thermal barrier coatings (TBCs) obtained from plasma sprayed stabilized zirconias have been reported previously by the authors of this article (Ref 6,7). These TBCs were also examined for their potential use in ceramic-coated diesel engines. It was found that significant improvement in fuel consumption efficiencies could be achieved with partial coating of engine components with such TBC material. The coatings were also found to be quite stable toward thermal cycling and the harsh physical and chemical environment in the diesel engines.

P. Ramaswamy and **S. Seetharamu,** Materials Technology Division, Central Power Research Institute, P.B. No. 8066, Bangalore 560 080, India; and **K.B.R. Varma** and **K.J. Rao,** Materials Research Center, Indian Institute of Science, Bangalore 560 012, India. Contact e-mail: kjrao@sscu.iisc.ernet.in.

Encouraged by the findings mentioned in the previous paragraphs, the potential of the naturally available zircon sand as a TBC material has now been examined. These fine sands can be readily sieved to obtain particles with a narrow distribution of sizes. The findings on plasma spray properties of these fine sand particles, chemistry of the resulting coatings subjected to thermal cycling, their thermal shock resistance, and their microstructures have been examined and are reported in this article. The studies suggest that zircon sand can be directly plasma spray coated, and the properties of the zircon coatings are very similar to those of stabilized zirconias. The elimination in this process of the expensive stage of preparation of plasma sprayable stabilized zirconia is considered very important for its indicated application.

2. Experimental Procedure

Zircon sand (naturally available) and yttrium oxide fine powder (99.9%) supplied by Indian Rare Earths Ltd. were used as starting materials for the preparation of the coatings. An 80 kW PlasmaTechnik spray system was used in the present work. Stainless steel plates, 100 by 100 by 3 mm, were employed as substrates to spray coat the sand. They were grit blasted with

Table 1 Spray parameters used in plasma spraying of zircon sand

Spray parameters	Value
Argon flow rate, L/min	35
Hydrogen flow rate, L/min	12
Powder gas flow rate (argon), L/min	3.2
Current, A	600
Voltage, V	71
Nozzle/electrode diameter, mm	6
Injector diameter, mm	1.5
Injector angle	90°
Injector distance, mm	6
Powder feed rate, g/min	50
Spray distance, mm	120

The substrate was air cooled during spraying.

Al_2O_3, degreased, and then spray coated with a 100 μm thick Ni22Cr10Al1.0Y bond coat (AMDRY 962). The zircon sand (ZS) and Y_2O_3 mixed zircon sand (ZS8Y) were then plasma sprayed according to the spray parameters given in Table 1. The ceramic was spray coated to a thickness of ~250 μm.

The coatings were subjected to thermal shock tests by exposing them to oxyacetylene flame with the open surface temperature of the coating maintained at 1000 and 1200 °C. The temperature on the ceramic surface and the metal was measured by using a K-type (chromel-alumel) thermocouple and an optical pyrometer. The fluctuation in surface temperature was approximately ±20 °C. The details of the tests have been reported elsewhere (Ref 7). Thermal barrier property was evaluated by measuring the temperature of the metal substrate when the surface of the coating was at 1000 °C and thereby obtaining the temperature drop across the ceramic. Phase analyses of the coatings were carried out by x-ray diffraction (XRD) studies. Scanning electron microscopy (SEM) and energy dispersive x-ray analyses (EDX) were used to determine the microstructures and chemical compositions respectively. Percentage porosity and particle/grain sizes and shapes were measured using image analysis of scanning electron micrographs (taken over five to six different regions).

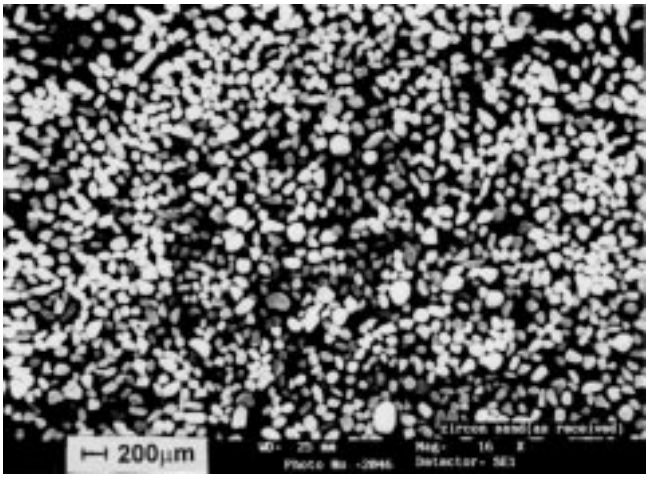

Fig. 1 Scanning electron micrograph for as received zircon sand

3. Results and Discussion

Figure 1 shows a scanning electron micrograph of as-received ZS. Narrow particle size distribution associated with roundness is a stringent requirement for plasma sprayability (Ref 8). Table 2 gives the particle size distribution in terms of length, breadth, and roundness. The particles in the as-received ZS have a narrow distribution of sizes (although, a bit coarse), and their roundness is adequate for plasma spraying without any further processing. Table 3 gives the average chemical composition of the particles expressed as weight percentages of the constituents. Figure 2 shows the x-ray diffractograms of the sands and coatings. The XRD (Fig. 2a) together with the composition as determined by EDX confirm that the major component of the sand is only $ZrSiO_4$. A few impurity phases identified by EDX are also listed in Table 3. The molar ratio of SiO_2 to ZrO_2 is ideally 1 to 2 in $ZrSiO_4$. The EDX analysis reveals that the ratio is 1 to 2.21, suggesting that excess ZrO_2 is present in the sand. However, presence of free $ZrO_2$was not indicated by the studies.

Natural sands have a geological history, and their surfaces are subjected to repeated washings by rain and running water. Therefore, the surface compositions of these particles can be

Table 2 Size analysis of zircon sand particles

Length (a)		Breadth (b)			
Range in μm	Percent	Range in μm	Percent	Roundness (c)	Percent
75-125	15	65-95	25	0.95-1.10	15
125-175	43	95-125	54	1.10-1.25	46
175-225	15	125-155	21	1.25-1.40	21
225-250	6	…	…	1.40-1.70	18

(a) Length of the longest feret (feret corresponds to the horizontal length of the feature). (b) Length of the shortest feret. (c) A shape factor that gives a minimum value of unity for a circle

Table 3 Chemical composition of zircon sand

	Composition, wt%								
		Region							
Compound	Average	1	2	3	4	5	6	7	8
ZrO_2	62.0	58.2	57.7	62.7	62.1	40.6	21.9	48.7	60.1
HfO_2	8.0	7.7	8.8	6.0	7.5	7.2	8.7	7.1	6.2
SiO_2	28.0	30.2	29.2	29.3	29.3	33.2	42.0	32.5	31.3
Al_2O_3	1.2	2.2	3.5	1.6	1.1	7.3	16.2	8.4	1.7
TiO_2	0.2	0.4	0.1	…	…	1.9	1.0	0.6	0.3
Fe_2O_3	0.2	0.8	0.7	0.4	…	8.7	7.1	2.1	…
CaO	0.4	0.1	…	…	…	0.3	0.7	0.1	…
MgO	…	0.1	…	…	…	0.8	2.5	0.4	0.4

Region numbers refer to those in Fig. 3. The standard deviations in the results are ±1%.

suspected to be different from that in the interior. Figure 3 shows the scanning electron micrograph of a freshly broken and exposed surface of a particle. It is evident that the interior of the sand particle is not homogenous. The interior regions were examined by EDX separately at several places (regions), and their compositions also are listed in Table 3. It can be noted that while the compositions of regions 1 and 2 are similar, regions marked 3 and 4 (regions that can be described as the outer shell of the particles) seem to be slightly rich in ZrO_2 (and definitely so if HfO_2 is also taken into consideration as a part of zircon composition). Regions 5, 6, and 7 are rich in alumina, and region 6 is particularly siliceous. The overall percentage of alumina (~16%) and silica (~42%) in region 6 is high. In other regions, the percentage of SiO_2 is only 29 to 32%. It is quite likely that the excess SiO_2 in region 6 (~12%) and the Al_2O_3 are in the form of aluminum silicates, an entire family of distinct materials (e.g., mullite, or Al_2O_3-SiO_2). It is highly difficult at present to ascertain the exact nature of the product formed. However, the ratio of Al_2O_3 to SiO_2, which is 58 to 42, suggests that the product may be a mixture of SiO_2 and mullite. Regions 5 and 6 are also rich in iron oxide. Region 8, closest to the periphery of the particle, is very similar to the surface composition. In general, the interior of the sand particles is not only heterogeneous in structure but also rich in silica or silicates. Thus, the surfaces of the sand particles appear to have been denuded of silicates during its natural history. Absence of magnesia and presence of only very low percentages of CaO and Al_2O_3 also support this view.

Figure 4 shows the scanning electron micrograph of as-sprayed surfaces of ZS coatings. Formation of a glassy phase is evident because it appears like a smooth splash, which has solidified on the surface. It has a nonuniform morphology with a distribution of significant porosity (up to ~10%). Smooth and well-rounded grains of varying diameters (20 to 100 μm) and

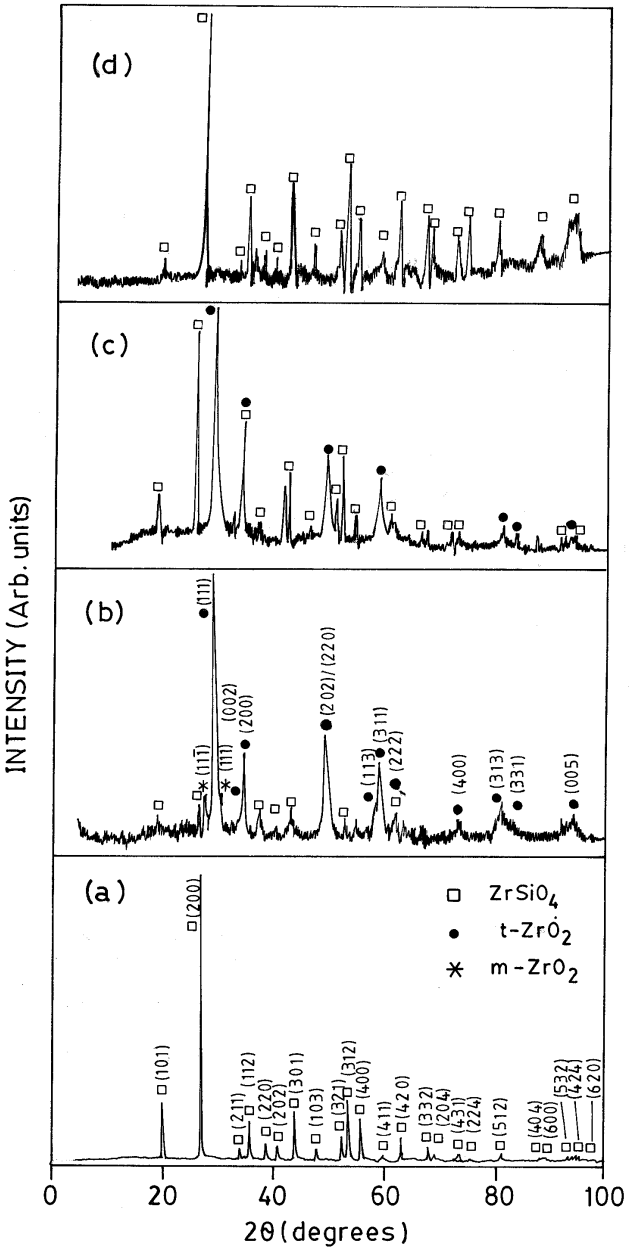

Fig. 2 X-ray diffractograms of the zircon sand and its coatings. (a) Zircon (as received). (b) Zircon coating (as-sprayed). (c) Zircon sand coating annealed at 1200 °C/1.44 × 10^4 s. (d) Zircon sand coating annealed at 1400 °C/1.44 × 10^4 s

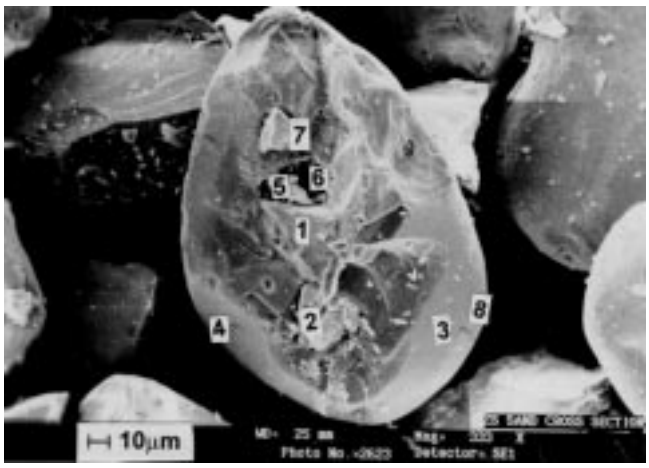

Fig. 3 Scanning electron micrograph of freshly broken and exposed surface of a zircon sand particle

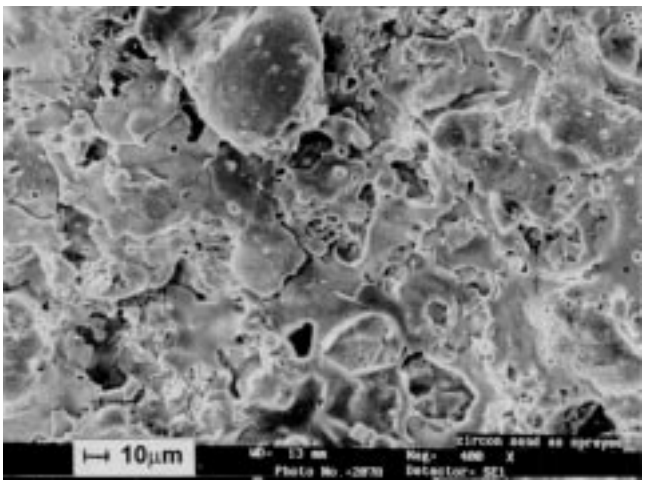

Fig. 4 Scanning electron micrograph of as-sprayed surface of a zircon sand coating

small regions, which are clearly clusters of fine particles (5 to 20 μm), are also visible in the micrograph. The structure and composition of the as-sprayed coating was determined using EDX and XRD. The interior and surfaces of some of the grains indicated a significant difference in composition. For example, grain interiors were rich in ZrO_2, while boundaries were rich in SiO_2 and other basic oxides (e.g., Al_2O_3, MgO, CaO, TiO_2, etc.). It immediately raises the suspicion that silicates with a low melting point have been there, which have melted and given rise to the liquid splash. The splash has quenched into a glass as a matrix making up most of the surfaces and the grain boundaries, whereas ZrO_2 (which contains HfO_2 and small amounts of divalent oxides CaO and MgO) constitutes much of the grain interiors. The XRD patterns shown in Fig. 2(b) confirm this feature. X-ray diffraction reveals that the single dominant crystalline phase in the coating is the t-ZrO_2. Small amounts of m-ZrO_2 and residual amounts of zircon are also present in the coatings. Thus, the Al_2O_3 and SiO_2 in the sprayed material must have formed the glassy phase. The amorphous nature of the as-sprayed ZS coating is also evident from the background of the XRD pattern shown in Fig. 2(b), where the base line is almost flat. The significant hump noticed in the as-sprayed and subsequently heat-treated specimens of both ZS and ZS8Y (shown in Fig. 2 and 5, respectively) indicates the presence of an amorphous phase in the product.

Comparison is readily made with the XRD of ZS given in Fig. 2(a) where the XRD peaks were all due to $ZrSiO_4$ only. The XRD together with EDX indicate that at the temperatures of the plasma, the sand is almost completely decomposed into its component oxides, t/m-ZrO_2, along with other oxides like SiO_2, Al_2O_3, CaO, and MgO, which readily form glass forming melts. The quenched spray coating, therefore, consists of phase-separated fine particles of ZrO_2 in a matrix of glassy alumino silicates. The micrograph in Fig. 4 shows that in some regions these particles form clusters.

The spray conditions are such that the recombination kinetics for ZrO_2 and SiO_2 to form $ZrSiO_4$ are expectedly very slow, and very little zircon could have reformed. Reformation of $ZrSiO_4$ has not been known to occur during fast cooling after the completion of the spray process (Ref 3). Similarly, because kinetics for phase segregation are also slow, ZrO_2 particles remain essentially very small in size (submicron) and are embedded in the matrix of silicate glass. Due to the small particle size and the consequent suppression of tetragonal → monoclinic phase transition, ZrO_2 is retained in its tetragonal phase in the sprayed coating. It can be noted here that t → m transformation of ZrO_2 is associated with an increase in volume (Ref 9) and is likely to be resisted by the hard alumino-silicate glass matrix. It is, however, possible that dissolution of MgO and CaO in ZrO_2 particles may also contribute to the stabilization of the tetragonal phase (Ref 10), although presence of a small proportion of m-ZrO_2 contradicts such a possibility.

3.1 Annealing Studies

The ZS coating was heated to 1200 and 1400 °C in two separate experiments and soaked at these temperatures for 1.44×10^4 s. This process of annealing of the coatings led to a remarkable recombination of SiO_2 and ZrO_2 to form $ZrSiO_4$. The x-ray diffractograms of the annealed coatings are shown in Fig. 2(c) and (d). On comparing the x-ray patterns shown in Fig. 2(a) and (d), the presence of $ZrSiO_4$ as the major phase in both the materials becomes evident. However, the presence of a significant hump in the pattern shown in Fig. 2(d) (unlike the flat background in Fig. 2a) indicates the presence of a matrix of amorphous nature. Evidently, the ceramic overlay retains the glassy nature of the matrix (attained during plasma spraying) even after heat treatment. The scanning electron micrograph of the coatings annealed at 1400 °C/1.44×10^4 s (Fig. 6) also has a very different appearance compared to the as-sprayed surface (Fig. 4). It is therefore clear that heating and annealing even for short duration is sufficient to induce ZrO_2-SiO_2 recombination. Two factors presumably promote the ZrO_2-SiO_2 reaction: (a) molten phase of silicates helps diffusion of Si^{4+} and (b) at t → m transition of ZrO_2 that may occur following the melting of the glass phase, reaction rate can increase to very high values due to the Hedvall effect (Ref 11).

The thermal barrier effect of the coatings should be expected to arise from the tetragonal phase of ZrO_2 (Ref 12). Nevertheless, this phase of ZrO_2 does not appear to be stable when the temperature of the coating exceeds the annealing temperatures, particularly for a long duration as in the present experiment (1.44×10^4 s). It was felt that deliberate stabilization of ZrO_2 in tetragonal phase by introduction of Y_2O_3 would be desirable. Zircon sand was mixed with Y_2O_3 in the proportion that would result in 8 wt% Y_2O_3 in the resulting ZrO_2. Well-mixed powders of ZS and Y_2O_3 were sprayed in the same manner onto steel plates previously coated with 100 μm thick NiCrAlY. Figure 7 shows the scanning electron micrograph of the surface of a ZS8Y coating. The appearance of the glassy splash is very similar to the as-sprayed coatings of the sands. The only significant difference is a number of small regions that appear to be clusters of fine (1 to 2 μm) particles. Energy dispersive x-ray analysis performed over the entire area provided an average composition that confirmed there is ~50% ZrO_2 but with a remarkably high percentage of Y_2O_3 (~30%). In the average composition SiO_2 was only ~18%, along with other oxides (Al_2O_3 and TiO_2) forming 2%. The region of clusters of fine particles, however, consisted of largely Y_2O_3 (93%) and a small percentage of the ZrO_2 (~6%) and other oxides (Al_2O_3 and SiO_2) constituting ~1%. The large concentration of Y_2O_3 observed in EDX may be due to the possibility that Y_2O_3 particles remained unreacted and unmelted in the plasma spray conditions and possibly bounced back to the top surface when the Y_2O_3 particles in the spray hit the substrate. The layer sticking to the bondcoat surface was evidently only the glass forming silicates.

Figure 5(a) shows the XRD pattern of a ZS8Y coating. In this pattern the Bragg peaks correspond to t-ZrO_2, Y_2O_3, and $ZrSiO_4$. It is clear that zircon has decomposed substantially giving rise to t-ZrO_2. Much of the added Y_2O_3 also appears to be present as a separate phase supporting the earlier observations from EDX.

These coatings were also subjected to thermal annealing at 1200 and 1400 °C, respectively, for 1.44×10^4 s in the same manner as ZS coatings. They were examined using XRD, SEM, and EDX. The XRD pattern obtained for 1200 °C/1.44×10^4 s annealed coating was quite similar to that of as-sprayed ZS8Y coatings. There was no evidence of recombination of ZrO_2 and SiO_2 (glassy phase). There was also no destabilization of t-ZrO_2.

Evidently, unlike in the case of Y_2O_3 free zircon (ZS) coats, in the sprayed product obtained in the presence of Y_2O_3, it is likely that the ZrO_2 phase was stabilized by Y_2O_3. It is however difficult to ascertain the extent of the incorporation of Y_2O_3 into the ZrO_2 from the present work. But the most surprising changes occurred when the coating was annealed for 1.44×10^4 s at 1400 °C. The XRD pattern (Fig. 5b) did not indicate the peaks corresponding to Y_2O_3 and $ZrSiO_4$. The presence of only t-ZrO_2 peaks suggests complete decomposition of $ZrSiO_4$ around this temperature. The scanning electron micrograph (Fig. 8) revealed well-formed grains with a microstructure very similar to that of Y_2O_3 stabilized sintered ZrO_2 ceramics (Ref 13). The grains were completely covered with a thin glaze. The EDX studies confirm that the composition of the surface of the coating was almost exclusively ZrO_2 (85%), Y_2O_3 (8 to 10%), and a small amount of SiO_2 (5%). It was therefore clear that the presence of SiO_2 was only confirming the expected composition of the thin glaze of the silicate glass covering the t-ZrO_2 particles. In fact, the EDX of the material collected from intergranular junctions revealed significantly high proportions of SiO_2 (up to 25%). Therefore at 1400 °C, all the Y_2O_3 dissolved in ZrO_2 and stabilized the tetragonal phase. The Y_2O_3 stabilized ZrO_2 seemed to be quite unreactive toward SiO_2. This was much unlike MgO stabilized ZrO_2, which destabilized at temperatures above 950 °C (Ref 14); and the destabilized ZrO_2 reacted with SiO_2 to form $ZrSiO_4$.

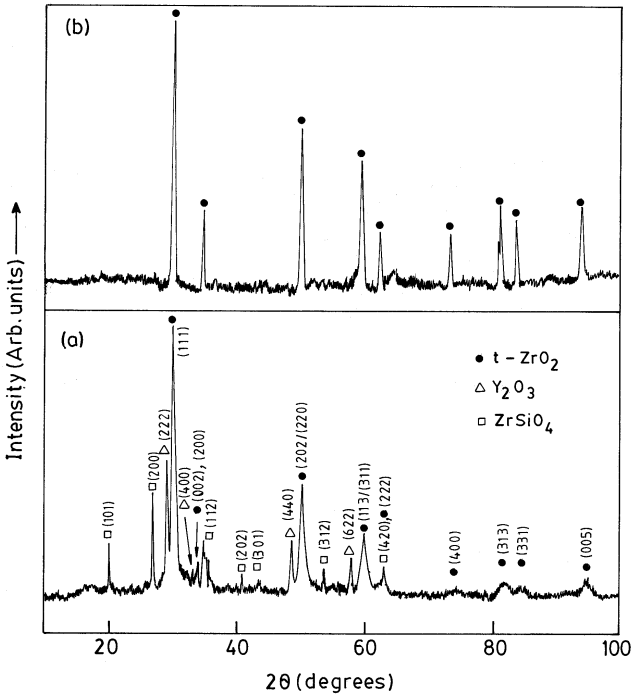

Fig. 5 X-ray diffractogram of ZS8Y coating. (a) As-sprayed. (b) Annealed at 1400 °C/1.44×10^4 s

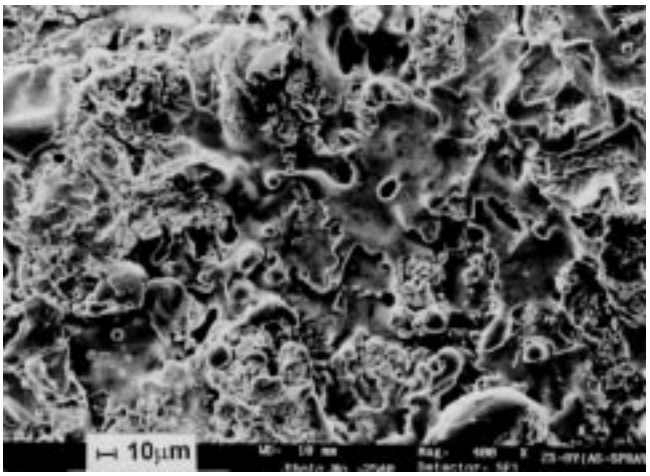

Fig. 7 Scanning electron micrograph of as-sprayed ZS8Y coating

3.2 Thermal Shock Resistance

Very vital to the applications of these coatings is their behavior in thermal shock cycling. In order to examine whether reactions seen under annealing experiments affect the thermal shock cycling behavior, both ZS and ZS8Y coatings were shock cycled from 1000 and 1200 °C. Observations were made after 275 such shock cycles. It can be noted that the shock cycles involved a

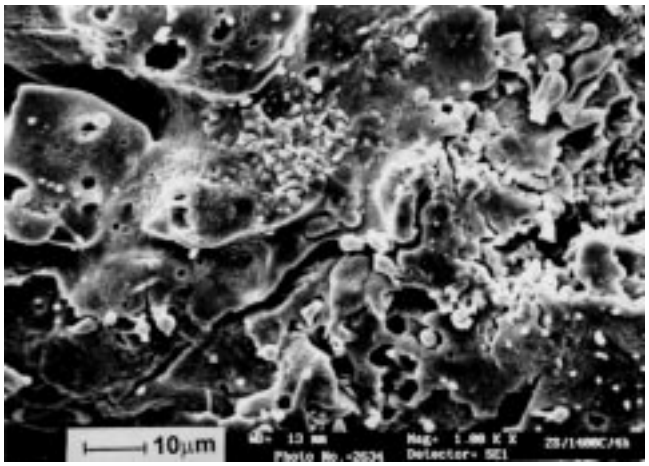

Fig. 6 Scanning electron micrograph of a zircon sand coating annealed at 1400 °C/1.44×10^4 s

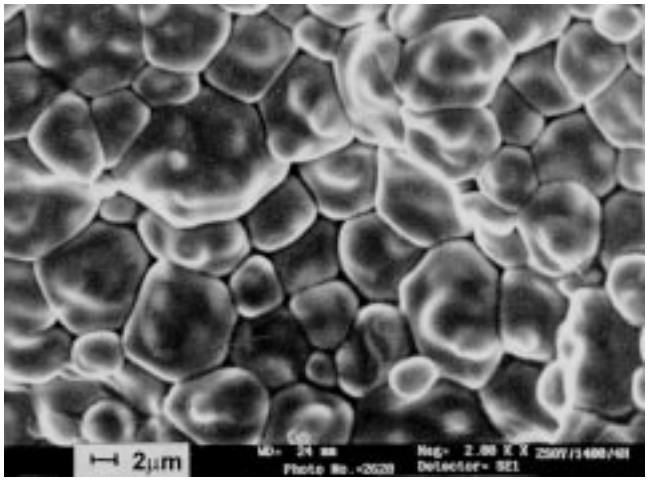

Fig. 8 Scanning electron micrograph of ZS8Y coating annealed at 1400 °C/1.44×10^4 s

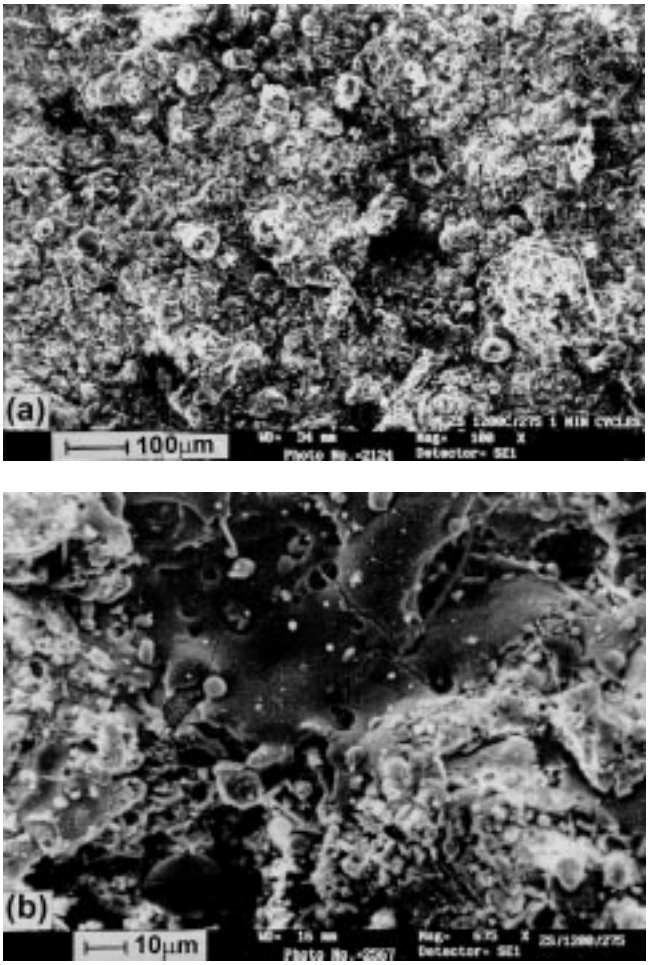

Fig. 9 Scanning electron micrograph of ZS coating after 275 thermal shock cycles between 1200 and <300 °C. (a) General surface. (b) Showing crack formation

holding time of 60 s at the high temperature (1000 or 1200 °C) and quenching to <300 °C in air for approximately 20 s. Thus in 275 cycles the cumulative soak time at 1000 or 1200 °C (~1.65×10^4 s) was greater than 1.44×10^4 s. However, the observations revealed that there was no change in the XRD patterns before and after shock cycling in the cases of both ZS and ZS8Y coatings. There was also no significant change in the SEM of both the coatings except that in the case of ZS coatings (Fig. 9a) where there was some amount of cavitation and crack formation (Fig. 9b). It is suspected that the crack formation could be due to gradual crystallization of silicates.

The silicate composition in the ZS coatings can be slightly richer in oxides of aluminum, calcium, magnesium, titanium, etc., than in ZS8Y coatings and therefore more prone to crystallization. The fact that in spite of a cumulative holding of 1.44×10^4 s at 1200 °C did not promote the same reactions as observed in direct annealing studies is surprising and still remains to be understood. It is felt that recombination reaction between ZrO_2 and SiO_2 particularly in ZS coatings is characterized by an induction time that is likely to be significantly greater than the 60 s for which the coatings were held at 1200 °C in every cycle. Therefore, the reactions were never really initiated and therefore, left the ceramic coating unaffected. Measurement of the surface temperature of the ceramic and the metal were carried out in the thermal shock cycling experimental setup. The flame was focussed continuously on the ceramic for 1800 s while steady state was being attained. The temperature differential between the metal and flame side was upward of 200 °C for a coating thickness of 250 μm. This again confirmed that the barrier effect is primarily due to the ZrO_2 phase in the coatings.

The ZS and ZS8Y coatings (particularly the latter) therefore provide an economically very advantageous route to making thermal barrier coatings. These coatings retain their integrity and all the important features of Y_2O_3 stabilized ZrO_2.

4. Conclusions

Both naturally occurring ZS and a combination of ZS and yttrium oxide have been plasma spray coated on bond coated stainless steel substrates. The t-ZrO_2 phase, which was formed on plasma spraying, substantially destabilized when the undoped ZS coatings were annealed at 1200 °C, followed by recombination of ZrO_2 and SiO_2 to form $ZrSiO_4$. The t-ZrO_2 phase however, was completely stabilized in the coatings of the ZS and Y_2O_3 mixture upon annealing at 1400 °C, and the coatings exhibited a microstructure similar to sintered Y_2O_3-stabilized ZrO_2 composition. Both the coatings exhibited good thermal shock resistance and thermal barrier characteristics, suitable for application as thermal barrier coatings. Direct use of ZS and its mixture with yttria therefore eliminates the expensive stage of preparation of plasma sprayable powders and results in coatings equivalent to that prepared from Y_2O_3-ZrO_2 plasma spray powders.

Acknowledgments

The authors thank the management of IISc and CPRI for the interest shown in the present work. The authors would also like to thank M/s Indian Rare Earths Ltd., Kerala, for providing the zircon sand used in the investigation.

References

1. R. Stevens, *An Introduction to Zirconia,* Magnesium Elektron Publication No. 113, 1984, p 20
2. A. Rudajevova, Thermal Properties of Plasma Sprayed $ZrSiO_4$, *Surf. Coat. Technol,* Vol 64, 1994, p 47-51
3. N.N. Ault, Characteristics of Refractory Oxide Coatings Produced by Flame Spraying, *J. Am. Ceram. Soc.*, Vol 40 (No. 3), 1957, p 69-74
4. K. Neufuss, P. Chraska, B. Kolman, S. Sampath, and Z. Travnicek, Properties of Plasma Sprayed Freestanding Ceramic Parts, *J. Therm. Spray Technol.*, Vol 6 (No. 4) 1997, p 434-438
5. P. Chraska, K. Neufuss, and H. Herman, Plasma Spraying of Zircon, *J. Therm. Spray Technol.*, Vol 6 (No. 4) 1997, p 445-448
6. P. Ramaswamy, S. Seetharamu, K.B.R.Varma, and K.J. Rao, A Simple Method for the Preparation of Plasma Sprayable Powders Based on ZrO_2, *J. Mater. Sci.*, Vol 31, 1996, p 6325-6332
7. P. Ramaswamy, S. Seetharamu, K.B.R.Varma, and K.J. Rao, *Evaluation of CaO-CeO_2 Partially Stabilized Zirconia Thermal Barrier Coatings,* Ceramics International, Vol 25, 1999, p 317-324
8. W.F. Calosso and A.R. Nicoll, Process Requirements for Plasma Sprayed Coatings for Internal Combustion Engine Components, *Energy-Sources Technology Conference and Exhibition,* (Dallas, TX),

15-20 February 1987, 87-1CE-15, American Society of Mechanical Engineers, p 1-8

9. E.C. Subbarao, Zirconia—An Overview, Science, and Technology of Zirconia, *Advances in Ceramics*, Vol 3, A.H. Heuer and L.H. Hobbs, Ed., American Ceramic Society, Inc., 1980, p 1-24
10. A.H. Heuer and M. Ruhle, Phase Transformations in ZrO_2-Containing Ceramics; I, The Instability of c-ZrO_2 and the resulting Diffusion-Controlled Reactions, Science, and Technology of Zirconia, *Advances in Ceramics*, Vol 12, N. Claussen, M. Ruhle, and A.H. Heuer, Ed., American Ceramic Society, Inc., 1983, p 1-32
11. C.N.R. Rao and K.J. Rao, *Phase Transitions in Solids*, McGraw Hill International, 1979
12. P. Vincenzini, Zirconia Thermal Barrier Coatings for Engine Applications, *Ind. Ceram.*, Vol 10 (No. 3), 1990, p 113-126
13. M. Matsui, T. Soma, and I. Oda, Effect of Microstructure on the Strength of Y-TZP Components, *Advances in Ceramics*, Vol 12, *Science and Technology of Zirconia II*, N. Claussen, M. Ruhle, and A. Heuer, Ed., American Ceramic Society, Inc., 1984, p 371-381
14. A. Bennett, Properties of Thermal Barrier Coatings, *Mater. Sci. Technol.*, Vol 2, 1986, p 257-261